PAPER

Check for updates

Hydrotalcite–PLGA composite nanoparticles for loading and delivery of danshensu

Lihui Pu, [ID] Haiyan Yu, Juan Du, Yanyan Zhang and Sihao Chen*

As one of the main pharmacodynamic components present in the water-soluble components of *Salvia miltiorrhiza* (Danshen), danshensu (DSS) is applicable to treating cardiovascular diseases. Nevertheless, such drawbacks as low water solubility and short half-life could reduce its bioavailability and restrict its clinical applicability. Therefore, it can be integrated into drug-carrying polymer microspheres, which is effective in improving the bioavailability of drugs. In this study, DSS was first embedded in a hydrotalcite (LDH) layer. Then, polylactic acid (PLGA) with excellent biocompatibility and biodegradability was coated on the surface. PLGA/DSS–LDH composite nanoparticles were prepared using the double emulsion (w/o/w) solvent evaporation method. As revealed by XRD and FTIR studies, success was achieved in embedding the drug DSS in the LDH layer, with the drug loading capacity of the LDH reaching 32.6%. A study was conducted on the encapsulation efficiency, surface morphology and *in vitro* drug release characteristics of PLGA/DSS–LDH. PLGA/DSS–LDH composite nanoparticles exhibited not only a high encapsulation efficiency but also a sustained release profile. The hemolysis assays demonstrated that the PLGA/DSS–LDH composite nanoparticles were ineffective in the induction of hemolysis, suggesting that PLGA/LDH composite nanoparticles can provide an effective controlled release drug system for pharmaceutics.

1. Introduction

Nowadays, cardiovascular disease remains the leading cause of death, accounting for about 35 per cent of global deaths each year.[1] In recent years, danshensu (SDSS) has attracted increasing attention due to its desirable effect in treating cardiovascular diseases. As one of the main pharmacodynamic components contained in the water-soluble components of *Salviae miltiorrhiza*,[2] SDSS is the sodium salt of danshensin and is capable of producing various pharmacological effects, for example, protecting cardiovascular and cerebrovascular systems, inhibiting tumors and reducing inflammation.[3] According to the relevant experimental results, DSS could repair hyperlipidemia and liver injury in mice by regulating the level of mRNA expression. DSS is able to suppress the development, migration and invasion of liver cancer cells by regulating the pi3k-akt signaling pathway. Moreover, DSS can inhibit adipogenesis through signaling pathways, thus reducing bone formation damage.[4]

Due to the high solubility and low permeability of DSS, however, its bioavailability is merely 11.09% and the oral elimination half-life lasts as little as 45.37 ± 9.23 min, which imposes a severe constraint on the clinical applicability of DSS.[5]

At present, most *Salvia miltiorrhiza* preparations on the market are quick-release formulations, which require patients to take medication more than three times per day, thus increasing the risk of side effects posed to the patients while making the long-term medication inconvenient for them. Therefore, it is absolutely necessary to design an effective method to extend the release time of danshensu, enhance its bioavailability, reduce its side effects on patients, and increase the convenience for patients to take medication. In order to extend the release time of DSS, there have been various methods proposed so far. For example, DSS sustained-release pellets were prepared to treat angina pectoris using the preparation method suggested by Panpan Yu *et al.* The ratio of DSS to sodium decanoate (SC) was optimized by single intestinal perfusion in rats. The DSS–SC-loaded pellet cores were prepared by means of extrusion–spheronization.[6] Nevertheless, this method is not only time-consuming but also less than satisfactory in producing the slow release effect. DSS capsules were prepared using a method devised by Danqing Wang *et al.* Tanshinone IIA (TA), tanshinol (TS), protocatechuic aldehyde (PD), salvianolic acid B (Sal B) sustained-release microspheres were first prepared and packed into capsules at their original weight ratio in pure *Salvia miltiorrhiza* extract.[7] However, it is inevitable for this approach to material decomposition to result in a certain degree of side effect on the human body. Therefore, it is imperative to find a way of extending the drug release time and reducing the potential side effects of medication on the human body.

College of Chemistry and Chemical Engineering, Shanghai University of Engineering Science, Shanghai 201620, People's Republic of China. E-mail: chensh@sues.edu.cn; Fax: +21 67791239; Tel: +86 21 67791239

In this study, it is proposed to prepare DSS as a controlled release drug. DSS was first combined with LDH to obtain DSS–LDH, which was then combined with PVA and PLGA to derive drug-carrying polymer microspheres. The drug-loaded polymer microspheres enable DSS to achieve multi-stage sustained release and extend the release time of the drug, thus enhancing the bioavailability of DSS and improving clinical outcomes. Compared with other DSS drug slow-release systems, LDH is classed as a naturally-derived substance in our drug carrier materials, experiments designed by Lins et al., MgAl/LDH-activated carbon composites. According to the experimental results, LDH performs well in loading the drug and leads to few side effects on human body.[8] A variety of polyester materials, such as polylactic acid and PLGA, demonstrate excellent stability and biocompatibility, which allows them to be metabolized by human body as normal and end up degrading into CO_2 and H_2O.[9,10] Therefore, controlled-release drugs are capable to reduce the side effects of drugs on human body. In line with Brzezinski design of experiment, PLA drug-loaded microspheres were prepared. According to experimental results, PLA is especially suitable for material, and the size of the drug-loading PLA microspheres is controllable.[11] Bode design of experiment demonstrated PLGA/PLA swelling orchestrates drug release. With regard to HME implants, the experimental results indicated that polymer swelling orchestrates the involved mass transport phenomena. It enables drug release after a certain lag time by making a significant change to the conditions for drug dissolution and coursing simultaneously.[12] These experimental results show that PLA and PLGA are good drug carrier materials and can play a role of drug slow release.

The layered structure of LDH contributes to high chemical versatility and anion exchange capacity, which makes LDH commonly used as adsorbents, catalysts, anion exchangers, flame retardants, polymer stabilizers, and so on.[13,14] In addition, LDH has also been applied as a delivery carrier in various medical and pharmaceutical applications.[15] The drugs that have been reported to use the drug-LDH sustained-release system include anti-inflammatory analgesics,[16,17] antitumor drugs,[18] cardiovascular drugs[19,20] and so on. LDH, as a new variety of drug carrier material, exhibits good safety, high biocompatibility and excellent biodegradability, which makes it effective in improving drug stability and curative effect, reducing the potential side effects, and achieving the delivery of sustained-release drug.[21] Compared with other DSS drug slow-release systems, LDH represents a naturally-derived substance in our drug carrier material. PLA and PLGA have good stability and biocompatibility, such polyester materials as PLA and PLGA can be metabolized as normal by human body and end up with degradation into CO_2 and H_2O,[22,23] which allows the controlled-release drugs to reduce the potential side effects of drugs on human body.

Therefore, this work is aimed at developing the PLGA/LDH composite nanoparticles loaded with DSS as an extended drug delivery system. DSS was first embedded in the LDH layer, and then PLGA/DSS–LDH composite nanoparticles were prepared using double emulsion (w/o/w) solvent evaporation method.

2. Experimental

2.1 Materials

PLGA ($M_w = 100\,000$ g mol^{-1}, PLA : PGA 50 : 50) was purchased from Jinan Daigang Biotechnology Co., Ltd. (China). SDSS was supplied by Xi'an Honson Biotechnology Co., Ltd (China). $Mg(NO_3)_2 \cdot 6H_2O$, $Al(NO_3)_3 \cdot 9H_2O$, NaOH, formamide and dichloromethane were obtained from Sinopharm Chemical Reagent Co. Ltd (Shanghai, China). All other chemicals required for the experiment were used as received.

2.2 Preparation of LDH

LDH with a 3 : 1 Mg/Al molar ratio was synthesized using co-precipitation method. $Mg(NO_3)_2 \cdot 6H_2O$ and $Al(NO_3)_3 \cdot 9H_2O$ were dissolved into CO_2-free deionized water, with the total metal cation concentration of the mixed salt solution set to 0.6 mol L^{-1}. The mixed salt solution was vigorously stirred under N_2 atmosphere at 40 °C. In the meantime, 1.2 mol L^{-1} NaOH solution was slowly dropped to maintain the pH value of the solution at about 10.0. Then, stirring was continued for 2 h under a N_2 atmosphere prior to aging for 8 h at 80 °C. Afterwards, the solution was cooled, filtered and washed with CO_2-free water to pH = 7. Finally, the obtained product was vacuum dried at 80 °C for 24 h. The resulting carrier was denoted as Mg_3Al–LDH–NO_3 (LDH).

2.3 LDH exfoliation and preparation of DSS–LDH hybrids

0.3 g of LDH powder was dissolved into 100 mL of formamide, for 30 minutes of ultrasonic treatment to obtain a translucent colloidal suspension, which was centrifuged at 12 000 rpm for 10 minutes to remove the nonexfoliated LDH. 0.5 g of SDSS was dissolved into 20 mL of deionized water prior to dropwise addition into the above-mentioned LDH colloidal suspension under slow magnetic stirring. The mixed colloidal suspension was stirred at room temperature for 12 h (N_2 protection). Then, the mixed colloidal suspension was centrifuged at 8000 rpm for 5 minutes and washed with deionized water for 3 times. Finally, the obtained solid was freeze-dried and was labeled as DSS–LDH hybrids.

2.4 Preparation of PLGA composite drug-loadednanoparticles

In this study, double emulsion (w/o/w) solvent evaporation method was applied to prepare PLGA composite nanoparticles. 0.5 g of SDSS or DSS–LDH compounds were dissolved into 9.1 mL of 1% PVA solution for the development of internal aqueous phase. 0.25 g of PLGA was weighted and dissolved into 5 mL of dichloromethane to develop an oil phase. Under the context of ice bath, 0.5 mL of internal water phase was added to the oil phase, while the ultrasonic probe was emulsified for 1 minute to obtain the primary emulsion. The primary emulsion (w/o) was added dropwise to 35 mL of 0.1% PVA aqueous solution with external water phase for further emulsification before a double emulsion (w/o/w) was obtained by mechanical stirring at 2000 rpm for 15 minutes. The resulting double

emulsion was further stirred (400 rpm) for 4 h at room temperature until the organic solvent was completely evaporated. Then, it was centrifuged, washed with water for 3–5 times, and freeze dried. The resulting nanoparticles were stored at low temperatures and they were denoted as PLGA–DSS and PLGA/DSS–LDH, respectively.

2.5 Characterization

The change in interlayer structure of LDH and DSS–LDH were measured by X-ray diffraction (XRD) conducted on a wide-angle analyzer (D/max-2500 PC, Bruker) with a Cu Kα radiation (λ = 0.154 nm) at a scanning rate of $10°$ min^{-1} and the diffraction patterns were collected from 5 to $80°$ (2θ).

FTIR analysis of LDH, DSS and DSS–LDH was conducted by means of FTIR spectroscopy (Nicolet Nexus 370 FTIR). Spectra were taken in a range of 400–4000 cm^{-1}.

A TA SDT Q600 thermal analysis system was applied to collect thermogravimetric data, while the sample was heated from room temperature to $650°C$ at a rate of $10°C$ min^{-1} under a flowing stream of nitrogen.

The mean volume diameter, the size distribution of PLGA–DSS nanoparticles and PLGA/DSS–LDH nanoparticles were determined using a nanoparticle size potentiometer (ZETA-SIZER Nano-S90).

The morphologies of samples were observed using a scanning electron microscope (SEM) (SU8010, Hitachi, Japan) and a transmission electron microscope (TEM) (Tecnai G2 F20, FEI, USA).

2.6 Loading of DSS on LDH

The drug loading of DSS–LDH nanohybrid was determined by spectrophotometer. 0.005 g of DSS–LDH was weighed and dissolved into 0.5 mL of 5 mol L^{-1} HCl solution. Then, the volume was fixed at 50 mL with deionized water. The absorbance was measured by TU-1901 UV-Vis spectrophotometer at 280 nm. After the concentration of DSS was determined according to the standard curve of the solution, the drug loading capacity of the LDH was determined to be 32.6%.

2.7 Drug loading and encapsulation efficiency of nanoparticle

15.0 mg of nanoparticles was weighed and dissolved using ultrasound into 0.5 mL of dichloromethane. Then, a certain amount of deionized water was added and sonicated until the dichloromethane was completely volatilized, which means polymer material was completely precipitated. Subsequently, the volume was fixed at 10 mL with deionized water, and the supernatant solution was filtered using 0.22 μm Millipore filters. The filtered solutions were analyzed for drug content with the assistance of a UV-Vis spectrophotometer at λ_{max} = 280 nm. Encapsulation efficiency and loading efficiency were calculated according to eqn (1) and (2), respectively.

$$\text{Encapsulation efficiency (EE)} = \frac{\text{amount of total loaded drug}}{\text{total amount of drug}} \times 100 \tag{1}$$

$$\text{Loading efficiency (LE)} = \frac{\text{amount of total loaded drug}}{\text{total amount of nanoparticles}} \times 100 \tag{2}$$

2.8 *In vitro* drug release

The release of DSS from DSS–LDH, PLGA–DSS and PLGA/DSS–LDH was constructed in PBS at pH 7.4 and pH 4.7, the absorbance of DSS at 280 nm using a 752N UV-Vis spectrophotometer (Jingke Industrial Co., Ltd., Shanghai, China). A sample weighing 20 mg was placed in a dialysis bag containing 1 mL of PBS. The dialysis bag was immersed in centrifuge tube containing 50 mL of PBS, which was incubated in an incubator shaker at a shaking speed of 100 rpm with the temperature range of 37 ± 0.5 °C. 10 mL of the samples was taken out at regular intervals and the same amount of fresh PBS was added promptly. The cumulative release of DSS (W) was calculated using eqn (3):

$$W\% = m/M \times 100 \tag{3}$$

where m represents the mass of DSS in the solution at specified time points and M refers to the mass of DSS in the solution at infinite time.

2.9 Hemolysis assays

The *in vitro* hemolytic behavior of the samples was measured to determine their biocompatibility, which plays a significant role in the circulation and distribution of PLGA/DSS–LDH nanoparticles in human body. Fresh blood collected from rabbits was anticoagulated with heparin for further use to evaluate the blood compatibility of all samples collected. The plasma was removed by centrifugation (3000 rpm, 10 min). Then, the red blood cells (RBCs) were washed 3 times with PBS at pH 7.4, before the RBCs collected by centrifugation were diluted with PBS to a concentration of 10% (v/v). Afterwards, 0.3 mL of the diluted RBCs was mixed with 1.2 mL of the samples at different concentrations (25–600 μg mL^{-1}). Distilled water and PBS were taken as positive and negative controls, respectively. The mixtures were incubated at 37 °C for 2 h. Finally, the samples were centrifuged (3000 rpm, 10 min) and the absorbance of supernatant at 541 nm was obtained using a microplate reader. The percentage of hemolysis of the samples was calculated by the following formula:

$$\text{Hemolysis} = \frac{A_S - A_N}{A_P - A_N} \times 100\% \tag{4}$$

where A_S, A_P and A_N represent the absorbance of the sample, the absorbance of the positive control and the absorbance of the negative control, respectively.

2.10 Rabit boold

Rabbit blood was obtained from 7–8 weeks old rabbits provided by Zhongshan Hospital affiliated to Fudan University. All

animal procedures were performed in accordance with the Guidelines for Care and Use of Laboratory Animals of Fudan University and approved by the Animal Ethics Committee of Fudan University.

3. Results and discussion

3.1 Exfoliation behavior

The delamination process of LDH in formamide consists of two steps, which are rapid swelling and slow exfoliation. When LDH is added to formamide, the interlayer water molecules are rapidly replaced with formamide, and the interlayer spacing is enlarged for a swelling phase to develop.[24] Due to oscillation, mechanical agitation or ultrasonication, a transverse sliding force was imposed on the swollen phase and the LDH host layers were split up. The transparent colloidal solution (Fig. 3a) obtained by the treatment of $Mg_3Al–LDH–NO_3$ with formamide, and the obvious Tyndall effect was observed with a side incident beam, suggesting that the presence of exfoliated LDH layers (nanosheets) in formamide.[25] After the addition of DSS to the LDH colloidal suspension, the Tyndall effect dissipated, as shown in Fig. 3b. It is thus speculated that the electrostatic interaction between the carboxylate of the DSS and the LDH nanosheet is stronger than the hydrogen bonding interaction between the carbonyl of the formamide and the LDH nanosheet. DSS anion and LDH nanosheet were restacked to generate DSS–LDH.

3.2 Intercalation of DSS into LDH layers

3.2.1 XRD analysis. The X-ray diffraction (XRD) patterns of LDH–NO_3 and DSS–LDH hybrids are shown in Fig. 4a. As revealed by the XRD pattern of the pristine LDH–NO_3 sample, all peaks are indicative of a well-crystallized hydrotalcite-like structure. The basal spacing (d_{003}) of the LDH–NO_3 crystals is 0.84 nm.[26] With regard to the XRD pattern of DSS–LDH nanohybrid, it is seen clearly that the diffraction peak of 003 crystal plane of DSS–LDH nanohybrid shifts forward relative to the XRD diffraction pattern of LDH, with the interlayer spacing of 1.11 nm, which is significantly larger compared to LDH, indicating that DSS was embedded in the LDH layer. As the thickness of LDH is approximately 0.48 nm, the height of DSS–LDH interlayer guest gallery is 0.63 nm after deducting the thickness of LDH. The length, width and thickness of DSS anion are 1.14 nm, 0.54 nm and 0.10 nm, respectively, as calculated using the molecular mechanics method (Chemoffic 2004 calculation, approximation). It is thus concluded that DSS anions are close to layer surface in the layer through the electrostatic interaction between the carboxyl group and the layer plate. Judged on the size of DSS molecule and the channel height of nanometer hybrid products, the potential orientation of DSS molecule in LDH channel was inferred.

3.2.2 FTIR spectra. Fig. 4b presents the FTIR spectra of SDSS, LDH and DSS–LDH nanohybrids. As shown in Fig. 2b, the broad absorption band at 3469 cm^{-1} stems from the –OH group and the physically adsorbed water in the LDH layer. The band at 1384 cm^{-1} is attributed to the NO_3^- stretching vibration. The strong band of pure SDSS at 1649 cm^{-1} and 1394 cm^{-1} is attributable to the stretching vibration of –COO^- and transits to 1685 cm^{-1} in DSS–LDH nanocomposites, which results from hydrogen bonding and the electrostatic interaction occurring between –COO groups and LDH layers. In addition, pure SDSS is the absorption peak of bending vibration in carbonyl plane at 1264 cm^{-1}, and the absorption peak of 1261 cm^{-1} appears in DSS–LDH nanohybrid as well due to the inserted DSS anion carbonyl plane bending vibration, which is similar to the
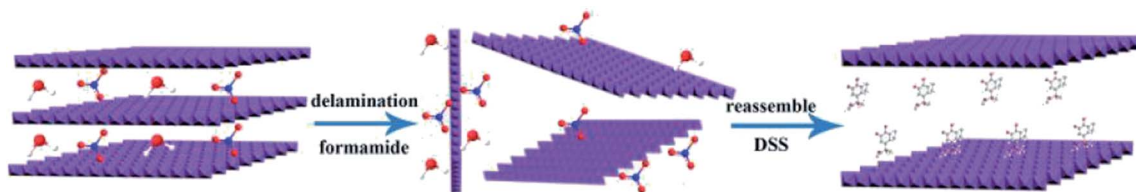

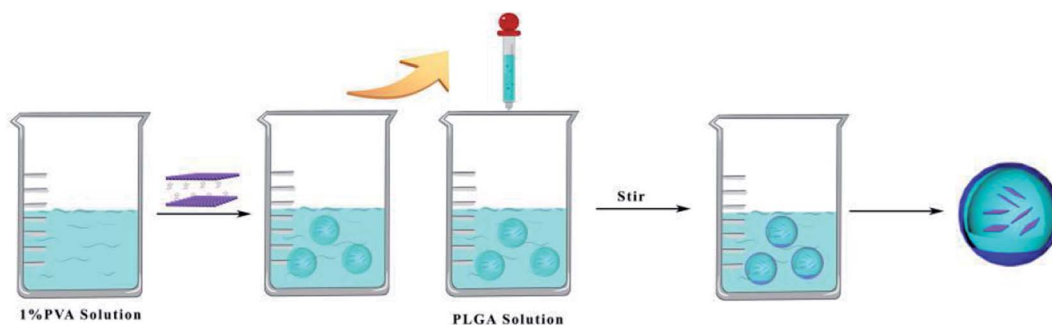**Fig. 1** LDH exfoliation and preparation of DSS–LDH hybrids.

Fig. 2 Preparation of PLGA composite drug-loaded nanoparticles.
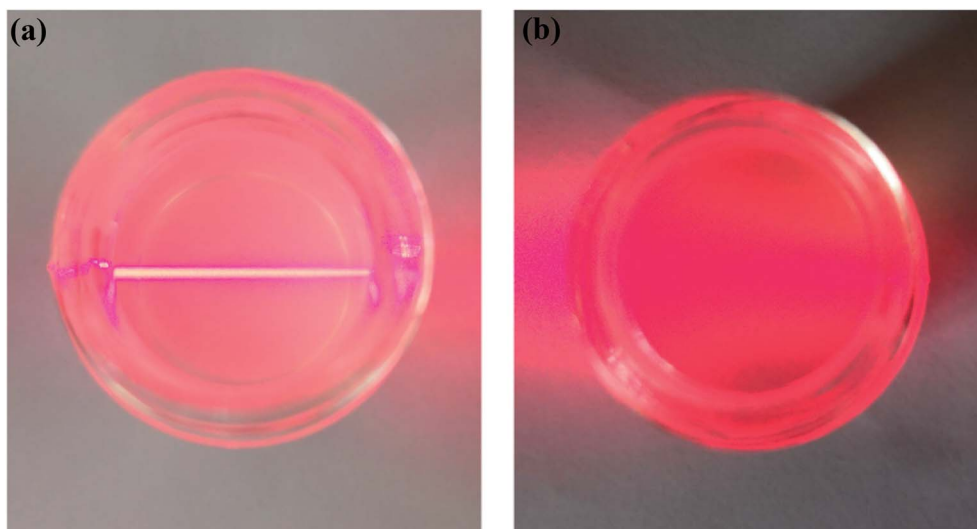
Fig. 3 Photographs of (a) colloidal suspensions of the exfoliated LDH and (b) the colloidal containing LDH and DSS.

corresponding SDSS. Moreover, it was observed that the intensity of characteristic absorption peak for nitrate at 1384 cm^{-1} in the precursor of LDH was significantly reduced, suggesting the exchange of nitrate.

3.2.3 TG-DSC analysis. DSS, LDH and intercalated product DSS–LDH were analyzed by means of thermogravimetric

analysis (TG) and differential scanning calorimetry (DSC). The TG-DSC curves of DSS, LDH and DSS–LDH nanohybrid samples are shown in Fig. 4c and d. For the LDH sample, there are two well-differentiated weight reduction steps in TG curve observed. In the first step, the total weight is reduced by roughly 11% from about 25 to 220 °C, which can be attributable to the loss of
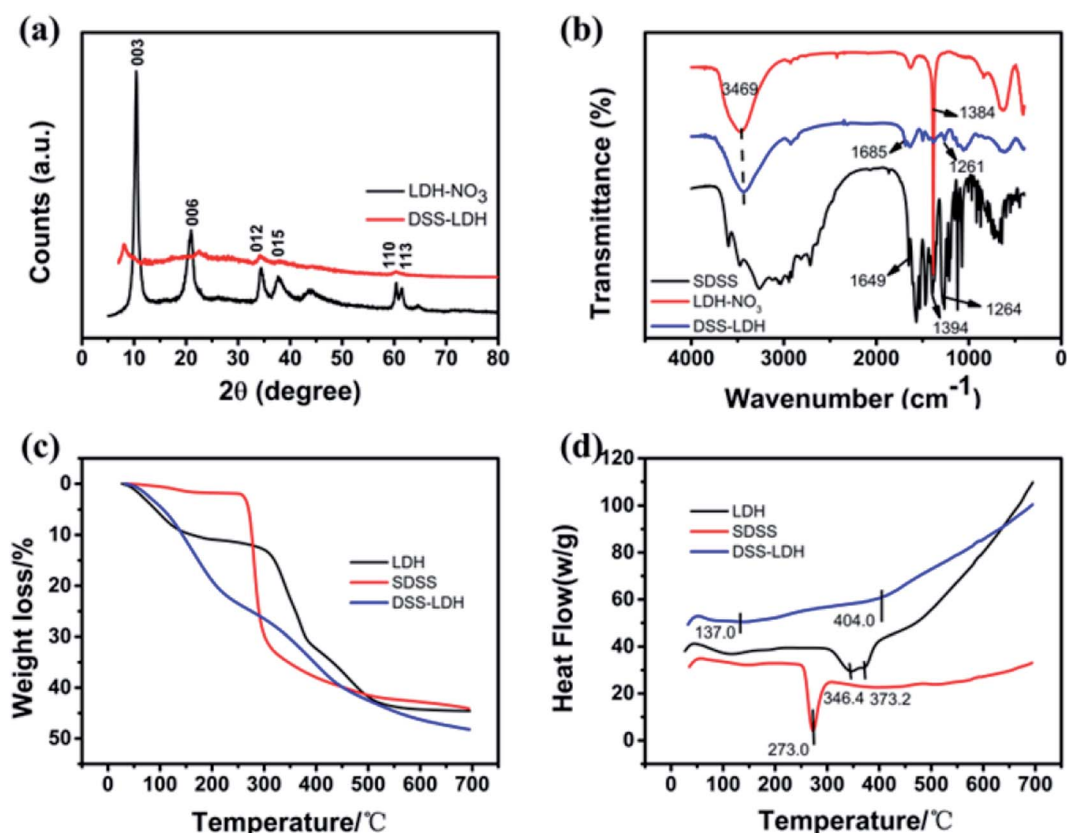

Fig. 4 (a) XRD patterns of LDH−NO$_3$, DSS−LDH hybrid; (b) FTIR spectra of LDH−NO$_3$, DSS−LDH hybrid and pure SDSS; (c and d) TG-DSC curves of LDH−NO$_3$, pure DSS−Na and DSS−LDH hybrid.
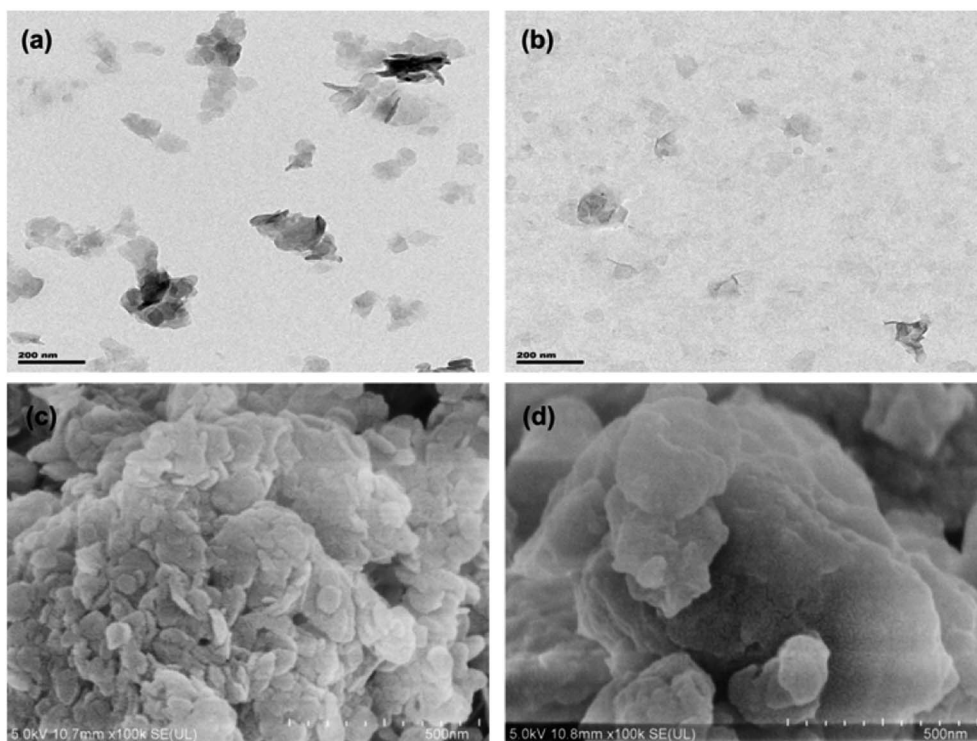
Fig. 5 TEM images of (a) LDH−NO₃, (b) the delaminated LDH and SEM images of (c) LDH−NO₃, (d) DSS−LDH hybrid.

physically adsorbed water and partial interlayer water. The second step occurs between 310 and 500 °C with a weight loss of 34%, which is potentially associated with the dehydroxylation of the layers and the decomposition of nitrate.[27] As for pure DSS, thermal decomposition (45% weight loss) was achieved at around 280 °C. As for DSS–LDH nanohybrid, there is a 9%
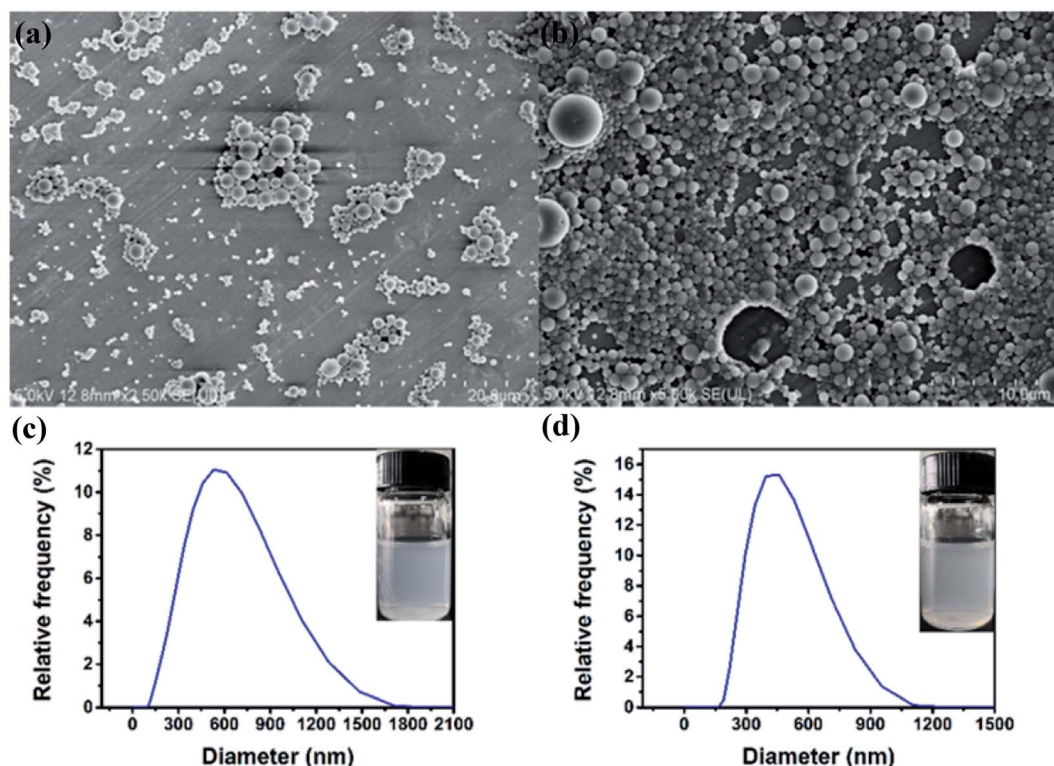

Fig. 6 SEM images of PLGA−DSS nanoparticles (a) and PLGA/DSS−LDH nanoparticles (b); particle size distributions of PLGA−DSS nanoparticles (c) and PLGA/DSS−LDH nanoparticles (d).
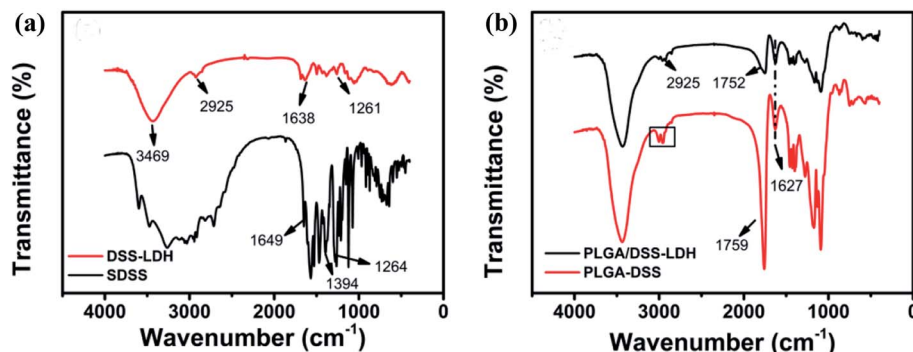
Fig. 7 FTIR spectra of (a) DSS–LDH hybrid and pure SDSS; (b) PLGA–DSS and PLGA/DSS–LDH.

weight loss between 20 and 120 °C, which is related to the loss of surface physically adsorbed water. It is suspected that the weight loss of about 15% between 150 °C and 280 °C results from the removal of interlayer water and the decomposition of surface adsorption DSS. The weightlessness occurring between about 330 °C and 600 °C is associated with the dehydroxylation of the layers and decomposition of interlayer DSS. Upon a comparison drawn with the decomposition temperature of pure DSS (about 280 °C), it can be judged that the thermal stability of intercalated DSS is significantly enhanced. The similar results were also observed for the intercalation of ibuprofen into LDH.[28]

3.2.4 Morphology analysis. The TEM images of LDH–NO$_3$ and the delaminated LDH are presented in Fig. 5. It was observed that the LDH–NO$_3$ particles existed in the form of hexagonal platelets with their size ranging from 50 to 100 nm and the delaminated LDH exhibited a particularly weak feature with a size ranging from 30 to 80 nm, which conforms to a typical feature of exfoliated nanosheets.[29] The SEM images of LDH–NO$_3$ and DSS–LDH nanohybrid samples are shown in Fig. 3. In addition, it was found out that the LDH–NO$_3$ particles exhibited a similar shape to hexagonal platelets. The DSS–LDH nanohybrid particles were shown to aggregate and a layered morphology remained visible after DSS insertion. Moreover, the surface of the nanohybrid particles showed an excellent smoothness, indicating the orientation arrangement and dense packing of the composed LDH nanosheets by preferential face-to-face and edge-to-edge aggregation.[30]

3.3 Drug-loaded PLGA composite nanoparticles

3.3.1 Morphology analysis. Fig. 6 shows the SEM images of PLGA–DSS nanoparticles and PLGA/DSS–LDH nanoparticles as well as the distributions of corresponding particle size. From Fig. 4a, it can be seen that the PLGA–DSS nanoparticles possess smooth surface and regular morphology, with no visible pores. In comparison with PLGA–DSS nanoparticles, the surface of PLGA/DSS–LDH composite nanoparticles shows a slightly higher roughness and more uniform distribution of particle size, as shown in Fig. 4b and d, which is potentially attributed to the diffusion of LDH crystals over the course of solvent evaporation. More LDH crystals break through the wall of the sphere to form pores on the surface, thus leading to the formation of a porous surface structure. The PLGA–DSS and PLGA/DSS–LDH nanoparticles show an average volume diameter of 565.05 ± 26.21 nm and 463.49 ± 26.79 nm, respectively, with their size distributions shown in Fig. 4c and d.

3.3.2 FTIR spectra. Fig. 7 presents the FTIR spectra of PLGA nanospheres. The FTIR spectra of SDSS and DSS–LDH nanohybrids are shown in Fig. 7a, while the FTIR spectra of the nanoparticles PLGA–DSS and PLGA/DSS–LDH are shown in Fig. 7b, where the absorption peak of –O–CH$_2$– is denoted as "□", which is the characteristic absorption peak of GA; at 1752 cm^{-1} and 1759 cm^{-1} are the C=O stretching vibration

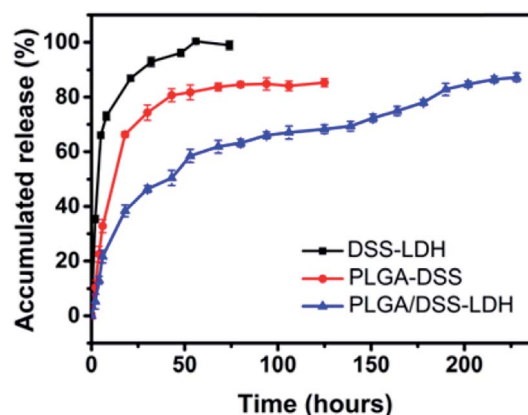**Table 1** Loading efficiency (LE) and encapsulation efficiency (EE) in DSS-loaded PLGA nanoparticles with different $V_{internal}$ to V_{oil} ratios

	$V_{internal}$/mL	V_{oil}/mL	LE/%	EE/%
DSS–LDH	0.1	5	0.54 ± 0.02	84.5 ± 3.1
	0.3	5	0.84 ± 0.01	45.5 ± 0.7
	0.5	5	1.73 ± 0.05	60.5 ± 2.1
DSS	0.1	5	0.5 ± 0.01	78.6 ± 1.6
	0.3	5	0.79 ± 0.07	42.1 ± 3.6
	0.5	5	1.32 ± 0.04	40.7 ± 2.3

Fig. 8 *In vitro* drug release curves of DSS–LDH, PLGA–DSS and PLGA/DSS–LDH.
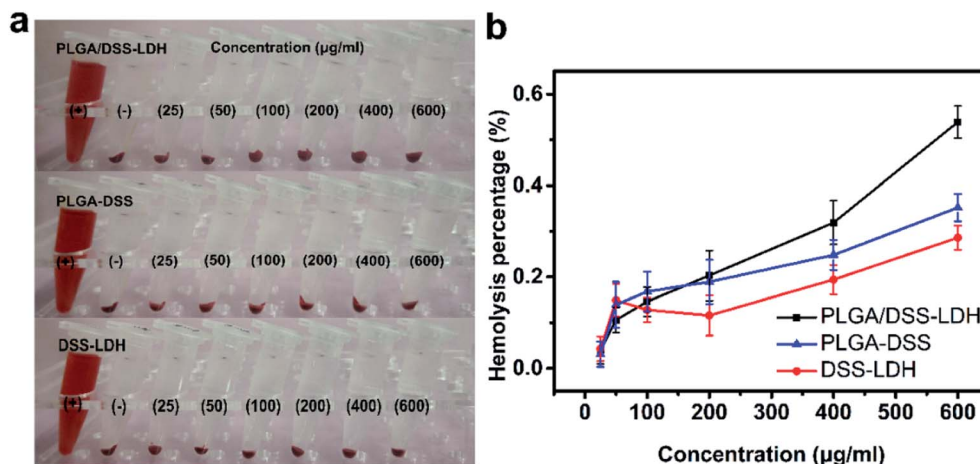
Fig. 9 Red blood cells (RBCs) hemolysis assay of DSS–LDH, PLGA–DSS and PLGA/DSS–LDH at different concentrations ((a) photographic images for direct observation of hemolysis by test samples; (b) hemolysis percentages of RBCs after test samples exposure, using distilled water and PBS as positive (+) and negative controls (−), respectively.).

peaks of PLGA.[31] The absorption peak of nanoparticles at 1627 cm^{-1} is the anti-symmetric stretching vibration absorption peak of –COO$^-$, which is potentially ascribed to the introduction of SDSS, and the absorption peak at 2925 cm^{-1} is observed in the FTIR spectra of PLGA/DSS–LDH and DSS–LDH, implying the success in the encapsulation of SDSS and DSS–LDH in the nanoparticles.

3.3.3 EE and LE. The EE and LE of the PLGA nanoparticles are detailed in Table 1. As the proportion of internal water phase is on the increase (equivalent to the increase of the amount of DSS), an incremental increase in the amount of DSS loaded can be observed. Similar results have been reported in other studies.[32] In addition, it was found out that EE exhibited a decreasing trend as the proportion of DSS in the stock solution of the sample increased with the internal water phase. When PLGA was loaded with DSS as a secondary controlled-release, the drug EE was 84.5%, 45.5% and 60.5%, respectively. In comparison, when PLGA was loaded with DSS as a primary controlled-release, the drug EE was 78.6%, 42.1% and 40.7%, respectively. Not only did the first-order controlled release ability of LDH improve the drug EE of the composite nanoparticles in the preparation process, it also prevented drug loss and improved the drug LE of the nanoparticles.

3.3.4 *In vitro* release of DSS. The release profile of DSS from the DSS–LDH, PLGA–DSS and PLGA/DSS–LDH when pH value is 7.4 are shown in Fig. 8. From Fig. 1, it can be seen that LDH loaded the drug DSS first and then integrated the DSS–LDH into PLGA matrix. The prepared DSS–LDH composite nanoparticles were clearly superior to PLGA nanoparticles loaded DSS directly *in vitro* drug release performance. In the first stage, the initial burst release of DSS was clearly observed in the samples of DSS–LDH and PLGA–DSS. Approximately 85% and 67% of DSS were released from DSS–LDH and PLGA–DSS within 20 h, respectively. In addition, the rapid release of DSS from DSS–LDH is speculated to result from the fact that DSS is a water-soluble drug capable to be quickly dissolved and released. By contrast, the burst release of PLGA–DSS is usually related to the

diffusion of the free or loosely bound drugs near the outer surface of the nanoparticles into the medium.[33] As revealed by the release profile of DSS from PLGA/DSS–LDH, the presence of LDH was effective in delaying the burst release of the drug, with approximately 40% of the DSS released in a space of 20 h. Additionally, a rapid process of drug release was observed after 150 h, which was potentially caused by a certain amount of medium penetrating into the particles, thus resulting in an increase of drug mobility.[34] Moreover, the composite nanoparticles exhibited a sustained release profile within 10 days and the cumulative release of DSS reached approximately 87%. It can be observed that placing the DSS–LDH in the nanosphere led to a multi-stage controlled release structure, which is conducive to slowing down the release of the drug.

3.3.5 Hemolysis assessment. Hemolysis test provides a method of contacting a sample with blood and measuring the amount of hemoglobin released from broken RBCs to evaluate the biomaterial for its blood compatibility.[35] The evaluation of plasma hemoglobin level reveals the cytotoxicity state caused by hemolysis and indicates the fragility of the red blood cell membrane when there is contact between blood and biomaterial.[36] Fig. 9 details the results of hemolysis test for the DSS–LDH, PLGA–DSS and PLGA/DSS–LDH at the concentrations ranging from 25 to 600 μg mL^{-1}. In Fig. 9b, it can be seen that there is almost an absence of hemolysis of RBCs detected in the samples of DSS–LDH, PLGA–DSS and PLGA/DSS–LDH, with the hemolysis percentages measured at the maximum concentration of 600 μg mL^{-1} being 0.286% ± 0.026, 0.352% ± 0.030 and 0.539% ± 0.035, respectively. These values are lower than the standard levels set out by ISO (reference < 5%),[35] indicating that these samples have no potential for hemolysis.

4. Conclusions

In this study, an attempt was made to develop an oral delivery system for the highly water-soluble drug danshensu. A combination of LDH–PLGA-based controlled drug delivery system for

oral administration of DSS was first proposed using the double emulsion (w/o/w) solvent evaporation method. The encapsulation efficiency, surface morphology and drug release characteristics of LDH–PLGA on drug DSS were examined and compared against PLGA–DSS nanoparticles. As indicated by XRD and FTIR studies, the drug SDSS was embedded in the LDH layer with success, with the drug loading capacity of the LDH reaching 32.6%. The presence of LDH in the PLGA matrix contributes to a longer path for the drug to be transferred from the interior of the nanoparticles to the external PBS buffer solution, thus reducing burst effects and leading to the sustained release behavior within 10 days. Therefore, it was demonstrated in the preliminary studies that the incorporation of LDH into the polymer biomaterial is effective in extending drug delivery, which contributed to a significant reduction in the frequency of administration and an improved patient compliance.

Conflicts of interest

The authors declare there are no conflicts of interest.

Acknowledgements

References

1 B. S. Schluter, B. Masquelier, C. J. E. Metcalf and A. Rasoanomenjanahary, *Glob. Health Action*, 2020, **13**, 13.

2 X. Y. Yuan, F. H. Fei, H. M. Sun, C. N. Xiao, X. F. Zhao, Y. J. Zhang and X. H. Zheng, *Int. J. Nanomed.*, 2018, **13**, 2265–2274.

3 T. Y. Li, Y. Chu, K. J. Yan, S. M. Li, X. Y. Wang, Y. Wang, W. Li, X. H. Ma, J. Yang and C. X. Liu, *Biomed. Chromatogr.*, 2017, **31**, 9.

4 Y. T. Li, Y. X. Chen, X. J. Huang, D. N. Huang, H. N. Gan, N. Yao, Z. X. Hu, R. Y. Li, X. Y. Zhan, K. F. Xie, J. Y. Jiang and D. K. Cai, *Lipids*, 2020, **55**, 127–140.

5 L. Zhou, M. S. Chow and Z. Zuo, *Int. J. Pharm.*, 2009, **379**, 109–118.

6 P. P. Yu, S. S. Zhang, W. L. Zhang, J. K. Yang, J. Lu and J. P. Liu, *Drug Dev. Ind. Pharm.*, 2017, **43**, 1093–1102.

7 D. Q. Wang, S. S. Zhang, H. Tang, C. P. Jiang, B. W. Wang and J. P. Liu, *Phytomedicine*, 2019, **58**, 9.

8 P. V. S. Lins, D. C. Henrique, A. H. Ide, J. L. D. Duarte, G. L. Dotto, A. Yazidi, L. Sellaoui, A. Erto, C. Zanta and L. Meili, *Colloids Surf., A*, 2020, **586**, 8.

9 R. Rojas and C. E. Giacomelli, *J. Mater. Chem. B*, 2015, **3**, 2778–2785.

10 C. Han, N. Cai, V. Chan, M. M. Liu, X. J. Feng and F. Q. Yu, *Colloids Surf., A*, 2018, **559**, 104–114.

11 M. Brzezinski, B. Kost, S. Wedepohl, M. Socka, T. Biela and M. Calderon, *Colloids Surf., B*, 2019, **184**, 8.

12 C. Bode, H. Kranz, A. Fivez, F. Siepmann and J. Siepmann, *J. Controlled Release*, 2019, **306**, 97–107.

13 Z. P. Xu, G. S. Stevenson, C.-Q. Lu, G. Q. M. Lu, P. F. Bartlett and P. P. Gray, *J. Am. Chem. Soc.*, 2006, **128**, 36–37.

14 Y. Yuan and W. Shi, *Appl. Clay Sci.*, 2012, **67–68**, 83–90.

15 V. Rives, M. del Arco and C. Martín, *Appl. Clay Sci.*, 2014, **88–89**, 239–269.

16 S. B. Khan, K. A. Alamry, N. A. Alyahyawi and A. M. Asiri, *Int. J. Nanomed.*, 2018, **13**, 3203–3222.

17 X. Lu, L. Meng, H. Li, N. Du, R. Zhang and W. Hou, *Mater. Res. Bull.*, 2013, **48**, 1512–1517.

18 Y. F. Zhang, X. W. Wu, Y. W. Mi, H. P. Li and W. G. Hou, *J. Phys. Chem. Solids*, 2017, **108**, 125–132.

19 A. I. Khan, L. Lei, A. J. Norquist and D. O'Hare, *Chem. Commun.*, 2001, 2342–2343, DOI: 10.1039/b106465g.

20 H. S. Panda, R. Srivastava and D. Bahadur, *J. Phys. Chem. B*, 2009, **113**, 15090–15100.

21 D. Li, Y. T. Zhang, M. Yu, J. Guo, D. Chaudhary and C. C. Wang, *Biomaterials*, 2013, **34**, 7913–7922.

22 R. Rojas and C. E. Giacomelli, *J. Mater. Chem. B*, 2015, **3**, 2778–2785.

23 C. Han, N. Cai, V. Chan, M. M. Liu, X. J. Feng and F. Q. Yu, *Colloids Surf., A*, 2018, **559**, 104–114.

24 D. J. Liang, X. Peng, Y. N. Li, H. L. Wang and X. J. Yang, *Adv. Mater. Interfaces*, 2017, **4**, 8.

25 R. Ma, Z. Liu, L. Li, N. Iyi and T. Sasaki, *J. Mater. Chem.*, 2006, **16**, 3809–3813.

26 J. Wang, J. Zhou, Z. Li, Y. Song, Q. Liu, Z. Jiang and M. Zhang, *Chemistry*, 2010, **16**, 14404–14411.

27 J. L. Milagres, C. R. Bellato, R. S. Vieira, S. O. Ferreira and C. Reis, *J. Environ. Chem. Eng.*, 2017, **5**, 5469–5480.

28 R. Djaballah, A. Bentouami, A. Benhamou, B. Boury and E. H. Elandaloussi, *J. Alloys Compd.*, 2018, **739**, 559–567.

29 X. Wu, S. Wang, N. Du, R. Zhang and W. Hou, *J. Solid State Chem.*, 2013, **203**, 181–186.

30 P. Gunawan and R. Xu, *J. Pharm. Sci.*, 2008, **97**, 4367–4378.

31 G. Mohammadi, A. Nokhodchi, M. Barzegar-Jalali, F. Lotfipour, K. Adibkia, N. Ehyaei and H. Valizadeh, *Colloids Surf., B*, 2011, **88**, 39–44.

32 M. D. Seema, *Appl. Clay Sci.*, 2013, **80–81**, 85–92.

33 G. Wu, L. Chen, H. Li and Y. J. Wang, *Bio-Med. Mater. Eng.*, 2014, **24**, 751–756.

34 H. Gasmi, F. Danede, J. Siepmann and F. Siepmann, *J. Controlled Release*, 2015, **213**, 120–127.

35 Z. He and L. Xiong, *J. Macromol. Sci., Part B: Phys.*, 2011, **50**, 1154–1161.

36 M. R. Farag and M. Alagawany, *Chem.-Biol. Interact.*, 2018, **279**, 73–83.